PCCP

Experimental observation of molecular-weight growth by the reactions of o-benzyne with benzyl radicals

Journal:	*Physical Chemistry Chemical Physics*
Manuscript ID	CP-ART-06-2024-002560.R1
Article Type:	Paper
Date Submitted by the Author:	20-Aug-2024
Complete List of Authors:	Couch, David; United States Air Force Academy Marchi, Myrsini San; Sandia National Laboratories, Combustion Research Facility Hansen, Nils; Sandia National Laboratories, Combustion Research Facility

ARTICLE

Experimental observation of molecular-weight growth by the reactions of *o*-benzyne with benzyl radicals

Received 00th January 20xx,
Accepted 00th January 20xx

DOI: 10.1039/x0xx00000x

David E. Couch,[a,b] Myrsini M. San Marchi,[b] and Nils Hansen[b]*

The chemistry of *ortho*-benzyne (*o*-C_6H_4) is of fundamental importance due to its role as an essential molecular building block in molecular-weight growth reactions. Here, we report on an experimental investigation of the reaction of *o*-C_6H_4 with benzyl (C_7H_7) radicals in a well-controlled flash pyrolysis experiment using a resistively heated SiC microtubular reactor at temperatures of 800-1600 K and pressures near 25 Torr. To this end, the reactants *o*-C_6H_4 and C_7H_7 were pyrolytically generated from 1,2-diiodobenzene and benzyl bromide, respectively. Using molecular-beam time-of-flight mass spectrometry, we found that *o*-C_6H_4 associates with the benzyl to form $C_{13}H_{11}$ radicals, which decompose at higher temperatures via H-loss to form closed-shell $C_{13}H_{10}$ molecules. Our experimental results agree with earlier theoretical calculations by Matsugi and Miyoshi [*Phys. Chem. Chem. Phys.,* 2012, **14,** 9722-9728], who predicted the formation of fluorene ($C_{13}H_{10}$) + H to be the dominant reaction channel. At temperatures above 1400 K, we also observed the formation of $C_{13}H_9$ radicals, most likely the resonance-stabilized fluorenyl π-radical. Our study confirms that molecular-mass growth via the *o*-C_6H_4 + C_7H_7 reaction provides a versatile pathway for introducing five-membered rings, and hence curved structures, into polycyclic aromatic hydrocarbons.

Introduction

ortho-Benzyne (*o*-benzyne, *o*-C_6H_4) is an aromatic molecule with a strained -C≡C- triple bond. Its unique chemistry, which is driven by both aryne and biradical character (Scheme 1), has captured scientific interest since the last century.[1-3]

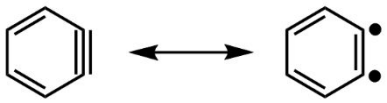

Scheme 1: *o*-Benzyne exhibits both aryne and biradical character.

o-C_6H_4 has been found in the high-temperature environments of combustion processes, where it is a product of thermal decomposition of phenyl radicals[4] and of larger hydrocarbons,[5] and it has been observed near molecular cloud TMC-1,[6] confirming expectations based on laboratory study.[7] It is therefore expected that *o*-C_6H_4 may play a significant role in combustion and astrochemical environments as a molecular building block for large polycyclic aromatic hydrocarbons (PAHs) and soot.[8]

o-Benzyne's potential role in molecular-weight growth has motivated experimental and theoretical kinetic studies of its reactions with radical and closed-shell species, to identify conceivable pathways to PAHs. For example, the *o*-C_6H_4 self-reaction has been studied experimentally several times.[9-11] The reaction between *o*-benzyne and benzene has been studied theoretically[12, 13] and experimentally[14, 15] and it is used as a comparison for reactions of *o*-benzyne with naphthalene and larger PAHs.[8] Additionally, reactions of *o*-benzyne with acetylene,[16, 17] ethylene,[16] propylene,[16] vinylacetylene,[18] cyclopentadiene,[4, 19] and methyl,[20] propargyl,[21, 22] allyl,[17] cyclopentadienyl,[4] and benzyl[22] radicals were studied experimentally and/or theoretically.

These reactions represent conceivable pathways to PAHs that are complementary to the commonly accepted molecular-weight growth mechanisms such as HACA (Hydrogen-abstraction-C_2H_2-addition),[23] PAC (phenyl-addition-cyclization),[12] and recombination of resonantly stabilized radicals.[24]

Identifying molecular-weight growth mechanisms remains an active area of research that has fascinated the physical chemistry community for many years,[25, 26] and evidence is accumulating that the reactions of *o*-C_6H_4 may play a significant role in the formation of five-membered ring structures. These chemical structures can contribute to molecular-weight growth via ring-enlargement reactions, are the building blocks of non-planar (curved) PAHs, and are responsible for the curvature of fullerenes and nanotubes.[27-29]

For example, five-membered ring compounds are predicted and/or shown to form from reactions of *o*-benzyne with methyl radical,[20] allyl radical,[17] cyclopentadienyl radical,[4] and cyclopentadiene.[4] Also, Matsugi and Miyoshi theoretically predicted that the reactions of *o*-C_6H_4 with propargyl and benzyl

[a] Department of Chemistry, United States Air Force Academy, CO 80840, USA
[b] Combustion Research Facility, Sandia National Laboratories, Livermore, CA 94550, USA
* corresponding author, email: nhansen@sandia.gov

Electronic Supplementary Information (ESI) available: [details of any supplementary information available should be included here]. See DOI: 10.1039/x0xx00000x

radicals lead to the five-membered ring structures fluorene and indenyl, respectively:[22]

$$o\text{-}C_6H_4 + C_7H_7 \rightleftarrows C_{13}H_{11} \rightleftarrows C_{13}H_{10}\ (\text{fluorene}) + H \quad (1)$$

$$o\text{-}C_6H_4 + C_3H_3 \rightleftarrows C_9H_7\ (\text{indenyl}) \quad (2)$$

These pathways are graphically summarized in Scheme 2. Matsugi and Miyoshi investigated the mechanisms and kinetics of reactions (1) and (2) using B3LYP and M06-2X methods and RRKM/master-equation calculations. Their calculations indicate that these reactions tend to form the fluorene ($C_{13}H_{10}$) and indenyl (C_9H_7) radical ring-structures. Shao *et al.* found these reactions to be important for PAH formation in a pyrolysis environment.[30]

Reactions of propargyl and benzyl radicals are themselves important and their roles in molecular weight growth have been studied extensively. It is understood that propargyl reactions dominate the formation of benzene, the smallest aromatic ring.[31] Propargyl reactions also contribute to the formation of five- and six-membered peri-condensed multi-cyclic species via the formation of aliphatically substituted aromatic intermediates.[32-34] Benzyl radicals can also form pericondensed ring structures through similar reactions, but are also important for PAH growth via the formation of aliphatically bridged PAHs.[35-38]

Following up on Matsugi and Miyoshi's earlier theoretical work,[22] we present here the complimentary experimental investigations for the reaction (1) of *o*-benzyne (o-C_6H_4) with benzyl (C_7H_7) radicals. We used a pyrolysis microreactor interfaced to a molecular-beam mass spectrometer for the detection of the temperature-dependent products of reaction (1). The reactants, *o*-benzyne and benzyl radicals, were produced in the reactor by co-pyrolysis of 1,2-diiodobenzene and benzyl bromide. We observed the predicted products and their decomposition products, highlighting simple pathways for introducing five-membered ring structures. To provide a benchmark and guidance for the interpretation of the data, we also studied the o-C_6H_4 + C_3H_3 reaction (2) via co-pyrolysis of 1,2-diiodobenzene and propargyl bromide. For this reaction, we confirmed in earlier experimental work[21] the theoretical predictions of Matsugi and Miyoshi[22] and identified the indenyl (C_9H_7) radical, the simplest radical species that consists of fused six- and five-membered rings, as the dominant reaction product of reaction (2).

Additionally, we provide qualitative comparisons between the cross reactions (1-2) and the respective self-reactions (3-5) of each reactant:

$$o\text{-}C_6H_4 + o\text{-}C_6H_4 \rightleftarrows C_{12}H_8 \quad (3)$$

$$C_7H_7 + C_7H_7 \rightleftarrows C_{14}H_{14} \quad (4)$$

$$C_3H_3 + C_3H_3 \rightleftarrows C_6H_6 \quad (5)$$

The reaction sequence elucidated here provides a versatile molecular-growth concept likely introducing five-membered ring structures into polycyclic aromatic systems. Such insights into the formation and understanding the reactivity of simple, prototypical five-membered ring structures are crucial for the development of a chemical description of molecular-weight growth.

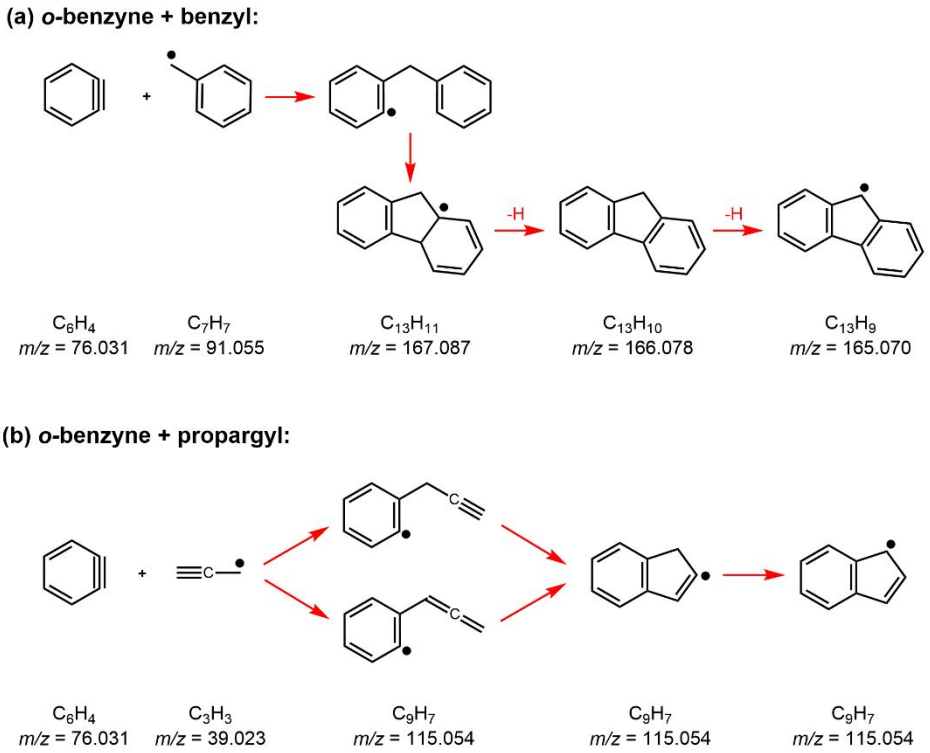

Scheme 2: Reaction pathways of o-C_6H_4 with benzyl and propargyl lead to formation of fluorenyl and indenyl radicals, respectively.

Experimental Setup

The experimental set-up used here is identical to the set-up used in our previous work on radical-radical chemistry.[32, 36, 39, 40] Only a short description is provided here. The experiment consists of a resistively heated silicon carbide (SiC) pyrolysis microreactor[41] (1 mm ID, 28 mm long) at a temperature range of 800-1600 K and ~30 Torr that is interfaced via a molecular beam to a reflectron time-of-flight mass spectrometer employing electron ionization. A flow rate of 50 sccm helium, with a small concentration of reactant precursors, passes through the microreactor into a high-vacuum chamber. The reactor temperature was monitored by a thermal camera (MicroEpsilon TIM M-1). The emissivity of SiC is assumed to be 0.82 but does not contribute substantially to the temperature measurement error of about 50 K.[42] The pressure profile inside the silicon carbide tube was determined by a boundary-layer flow simulation.[43] The simulated pressure profiles along with thermal camera images showing the temperature of the microtubular reactor are shown in the Supplementary Information. The observed inlet pressure is about 50 Torr, and the simulation indicates that the pressure at the hottest portion of the tube is about 30 Torr. The temperature profiles are similar to those reported previously.[32, 39]

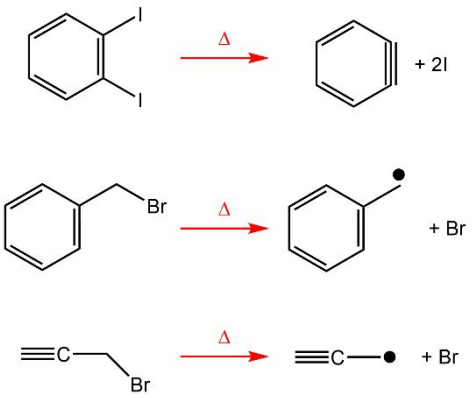

Scheme 3: Formation of *o*-C_6H_4, benzyl, and propargyl via flash pyrolysis of 1,2-diiodobenzene, benzyl bromide, and propargyl bromide.

We used 1,2-diiodobenzene ($C_6H_4I_2$), benzyl bromide (C_7H_7Br), and propargyl bromide (C_3H_3Br) as precursors for *o*-benzyne, benzyl, and propargyl, respectively (Scheme 3). The 1,2-diiodobenzene was added to the helium flow entering the pyrolysis reactor by flowing 37-40 sccm of He over liquid diiodobenzene contained in a vial held at 80°C using a hot water bath. The concentration of benzyne during the experiment was determined to be 0.1% in post-processing by weighing the sample vial before and after the experiment and assuming a constant rate of evaporation during the time helium was flowing. We have shown this to be a good approximation for other chemicals,[39] when we could not make real-time measurements.

Benzyl bromide was added by flowing 10 sccm He across a room temperature vial of benzyl bromide. Concentration of benzyl bromide was determined by measuring the rate of change of the liquid level in the vial. The flow was combined with the 40 sccm passing through the diiodobenzene vial for a total flow rate of 50 sccm.

Propargyl bromide was premixed in a stainless steel sample bottle. Propargyl bromide 80%wt in xylene was freeze-pump-thawed twice to remove air, then the sample bottle was filled to 25 Torr allowing the vial to get cold (around 10 °C) due to the evaporation. Xylene has a negligible vapor pressure at 10°C, so most of the sample is propargyl bromide. Then the sample bottle was filled to 3153 Torr with helium, for a concentration of 0.8%. The flow of propargyl bromide mix was 12.5 sccm during the experiment, which when combined with the 37.5 sccm flow through the diiodobenzene vial gives a total flow rate of 50 sccm and a 0.2% propargyl bromide concentration. The line pressure before the reactor was 30-60 Torr, rising with increasing temperature. At these pressures, we assume mixing occurs quickly in the supply line.

After passing the mixed gases through the heated SiC reactor, the gas stream exits into the source chamber at a pressure of ~10^{-3} Torr. The rapid pressure drop creates a gas expansion with limited rovibrational cooling that is likely not quite a supersonic molecular beam.[44] Since this work does not use spectroscopic information, the precise temperature of the beam is not considered further. The resulting gas jet is sampled through a 0.4-mm-diameter skimmer into the ionization chamber of the mass spectrometer. The mass spectrometer has been described in more detail previously.[45, 46] We used a heated tungsten filament to produce electrons with a tunable energy probability function characterized by a full width at half maximum (FWHM) of 2.2 eV. The data were recorded with a nominal electron energy of 12 eV to minimize ambiguities caused by dissociative ionization. The ions were mass-selected using their flight time in a reflectron configuration towards a microchannel plate detector and signals were recorded using a multichannel scaler. The instrument's mass resolution of $m/\Delta m$ ~3500 allows for the separation of the elemental composition in the considered mass range and the instrument's detection limit of ~1 ppm allows for sensitive detection of reaction intermediates.

The combination of the earlier synchrotron-based experiments for the *o*-C_6H_4 + C_3H_3 reaction[21] and the simplicity of the potential energy surface for the reaction studied here,[22] allows for meaningful experiments using the non-isomer-resolved electron ionization technique. For the purpose of this work, to provide experimental evidence for molecular-growth via the *o*-C_6H_4 + C_7H_7 reaction, determination of the exact isomeric distribution is not essential.

Additionally, wall reactions cannot be excluded given the dimensions of the SiC reactor and the pressure and temperature conditions. Reactions with soot buildup tend to decrease the concentration of radicals by donating hydrogens to these reactive species. The presence of such reactions does not change the conclusions of this study.

Results

In this section, we present the long-awaited experimental confirmation for Matsugi and Miyoshi's prediction of molecular-

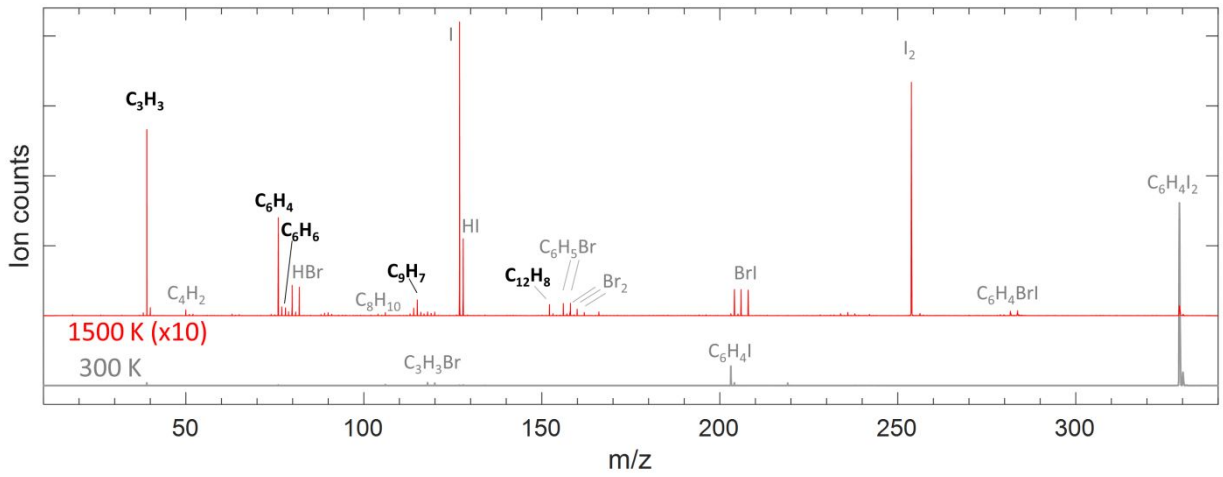

Figure 2. Mass spectra for the C_3H_3 + C_6H_4 reaction. Species of interest in this study are shown in bold black. Halogen side reactions create large signals due to the large ionization cross section of Br and I atoms.

weight growth through the formation of five-membered ring structures via the *o*-benzyne + benzyl reaction (1). In recent work,[21] we experimentally confirmed Matsugi and Miyoshi's prediction for the formation of five-membered ring containing indenyl radicals through the *o*-benzyne + propargyl reaction (2).

This latter reaction will be the starting point of the discussion presented here, supporting the interpretation of the experimental data on the targeted *o*-benzyne + benzyl reaction (1).

o-benzyne + propargyl

Figure 1 shows the mass spectrum of a cold-gas mixture of 1,2-diiodobenzene and propargyl bromide and the spectrum following the flash co-pyrolysis of those two precursors at 1500 K. This mass spectrum appears somewhat congested, but most of the signals correspond to side reactions of Br and I, both of which have large ionization cross sections (especially iodine). Focusing solely on the hydrocarbon products, we observe $C_{12}H_8$ (biphenylene), which is the expected product of the benzyne + benzyne self-reaction (3),[9, 11, 47] C_6H_6, which is the expected product of propargyl + propargyl self-reaction (5),[48, 49] and the cross-reaction product C_9H_7 from reaction (2). A small amount of xylene from the C_3H_3Br sample can be seen at *m/z* 106.078 (C_8H_{10}). C_4H_2 is a decomposition product of C_6H_4. In order to verify that the observed C_9H_7 is a product of the targeted cross reaction as opposed to a self-reaction, mass spectra of the pyrolysis of each reactant precursor individually are shown in the Supplementary Information for comparison.

Using the electron ionization method is this paper, we cannot determine the identity of the C_6H_4 isomer. Besides the cyclic *o*-benzyne, the linear 1,5-hexadiyne-3-ene might be formed through isomerization of *o*-C_6H_4 at temperatures around 1400 K.[50, 51] However, side reaction of the linear C_6H_4 isomers with radical species, *i.e.,* propargyl and benzyl, would need to occur through a barrier that is typical for molecule-radical reactions. Therefore, these reactions are likely much slower than benzyne-radical reactions and can thus be neglected.

Another problem with studying radical-radical reactions in these microtubular reactors is that the precursor decomposition reactions need to occur at the same (or similar) reaction temperature. It is shown here in Fig. 2 that both C_6H_4 and C_3H_3 precursors start to decompose to form the targeted precursor molecules around 1100 K, monotonically increasing with higher temperatures. For a reference, the C_9H_7 product starts to form around 1200 K, with a maximum reached at 1500 K.

Figure 2 shows the total ion count for the two reactants, C_3H_3 and C_6H_4, and for the main product C_9H_7. The C_3H_3 and C_6H_4 signals have been corrected for signal from dissociative ionization of the respective precursors $C_6H_4I_2$ and C_3H_3Br, using the assumption that the fragment branching ratios are independent of reactor temperature. These three species were not calibrated to absolute concentrations in this work due to the difficulty of producing a reliable standard. The observed ion counts are proportional to the species' concentration and furthermore, molecules similar in size and composition generally have similar electron ionization cross sections, thus allowing for a rough estimate of the beam composition. A

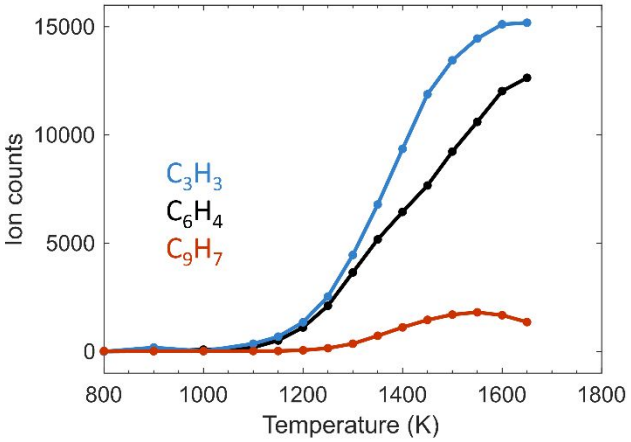

Figure 1. Integrated ion counts for the C_3H_3 and C_6H_4 precursors and the C_9H_7 product. Both reactants have similar temperature profiles, facilitating the cross-reaction. Dissociative ionization of the precursors has been subtracted from the raw C_3H_3 and C_6H_6 signals.

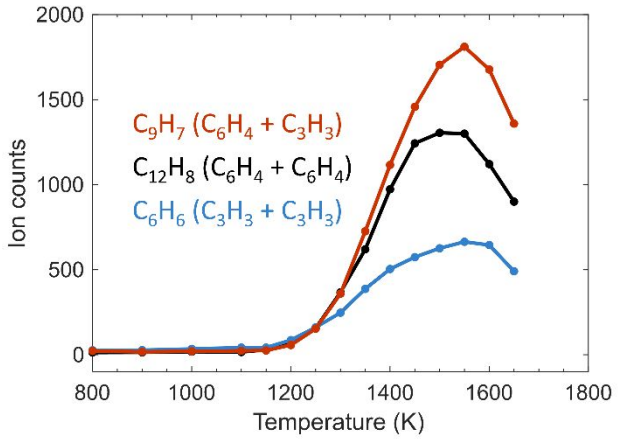

Figure 3. Comparison of the products of the self-reaction of C_6H_4 and C_3H_3 with that of the cross-reaction. The cross-reaction appears to be more favorable, though without calibration we cannot have a definitive determination.

calibration gas was used to confirm that all masses over this range have very similar temperature-dependent sampling efficiency, and that sampling efficiency increases with increasing temperature by about 70% over the temperature range of the experiment. (See Supplementary Information). This change is likely due to some changes in the reactor-skimmer-ionization region alignment caused by the temperature. The reactor was aligned with the skimmer at 1500 K by optimizing the pressure in the ionization chamber, and both the pressure in the ionization chamber and the ion signal of the calibration gas then decreased when cooling the reactor. Both precursors decompose into the desired reactants within the same temperature range, allowing these reactants to readily find each other without the need for a long lifetime. The temperature dependence of the C_9H_7 roughly follows the product of the reactant concentrations.

As expected from theory[22] and validated by earlier experiments,[21] the reaction of these reactants produce C_9H_7 (m/z 115.055). Matsugi and Miyoshi predict that a large part of the product is trapped in the deep well of the indenyl radical.[22] According to their work, the reaction proceeds through two isomeric initial intermediates (C_6H_4-CH_2CCH and C_6H_4-$CHCCH_2$) that are formed through *o*-benzyne association with the CH_2-side and CH-side approach of the propargyl radical, respectively. Because of the absence of a significant energy barrier, these initial adducts readily isomerize to a cyclopentenyl-fused benzene that subsequently forms the most stable C_9H_7 isomer, the indenyl radical (see Scheme 2).

A direct determination of the reaction rate is not feasible in the present experiment due to the difficulty of calibrating concentrations and the presence of side reactions. We can, however, gain some insight into the importance and relative rate of reaction (1) by comparing the signal strength of the cross-reaction product C_9H_7 to those of the self-reaction products, $C_{12}H_8$ and C_6H_6 (Figure 3). The cross-reaction product signal is the highest of the three for the full temperature range of interest, implying that this reaction competes favorably with the self-reactions, a necessary condition for this reaction to be of much significance in a flame or pyrolysis environment. Interpreting signal as concentration in this manner requires some further discussion. Ionization cross section and mass discrimination factor tend to increase for increasing molecular size, so it is likely that C_6H_6 is under-sampled and $C_{12}H_8$ is oversampled compared to C_9H_7. Also, C_9H_7 is a radical and could react further which would lower its concentration, but we do not see evidence of further reaction.

The detection of HI and HBr indicates the presence of hydrogen abstraction reactions. However, the likely co-products of these reactions were not observed, indicating that these H atoms may come from soot plated on the walls of the reactor. In past experiments on phenyl radicals using the same apparatus,[32, 36, 39] we consistently saw benzene presumably as a product of H-abstraction from the walls. In contrast, *o*-benzyne does not show this tendency to abstract H atoms.

In summary, the present results concerning the reaction of *o*-benzyne with propargyl are consistent with our earlier work,[21] both in the production of *o*-benzyne from the pyrolysis of 1,2-diiodobenzene and the formation of the expected C_9H_7 product. Based on the work, the C_9H_7 signal is interpreted as indenyl, *i.e.,* a five-membered ring structure.[21, 22] The results in this section add confidence in the interpretation of the *o*-benzyne + benzyl reaction discussed next.

o-benzyne + benzyl

A typical cold-gas mass spectrum for a co-flow of 1,2-diiodobenzene and benzyl bromide is shown in Fig. 4. The mass spectrum is dominated by the precursor molecules $C_6H_4I_2$ and C_7H_7Br and a corresponding dissociative ionization fragment at C_7H_7. During co-pyrolysis at 1500 K, the mass spectrum is more complex, showing evidence for the desired reactants, C_6H_4 and C_7H_7, and the targeted product at $C_{13}H_{10}$ (+H). Consistent with the previously described *o*-C_6H_4 + C_3H_3 reaction, products of the self-recombination reactions of C_6H_4 and C_7H_7 at $C_{12}H_8$, $C_{14}H_{14}$ and $C_{14}H_{12}$ were also detected. C_5H_5 is likely to be a product of thermal decomposition or dissociative ionization of species such as C_7H_7.[52, 53] As in Fig. 1, side reaction products involving Br and I, labelled in grey, appear prominently in the mass spectrum due to their large ionization cross sections. We note that the $C_{13}H_{9\text{-}11}$ products are only detectable when both precursors are present, indicating that they are formed in the targeted reaction (1).

The temperature dependence of the reactant signals C_6H_4 and C_7H_7 are shown together with the products $C_{13}H_{11}$, $C_{13}H_{10}$, and $C_{13}H_9$ in Fig. 5. Pyrolysis of only 1,2-diiodobenzene and pyrolysis of only benzyl bromide do not show these products (see SI), confirming that these are cross-reaction products. We paid particular attention to the potential formation of fluorene ($C_{13}H_{10}$) in the *o*-benzyne reaction network, as discussed by Hirsch *et al.*[11] However, the concentrations in our experiments were significantly lower, precluding the formation of fluorene in detectable amounts from 1,2-diiodobenzene pyrolysis alone.

For the *o*-C_6H_4 + C_7H_7 reaction, the temperature dependence of the reactants is not as well matched as for the *o*-C_6H_4 + C_3H_3 reaction. Nevertheless, significant overlap occurred allowing for a sufficient production of the targeted $C_{13}H_{9\text{-}11}$ products. Figure 5 shows that the benzyl radical appears

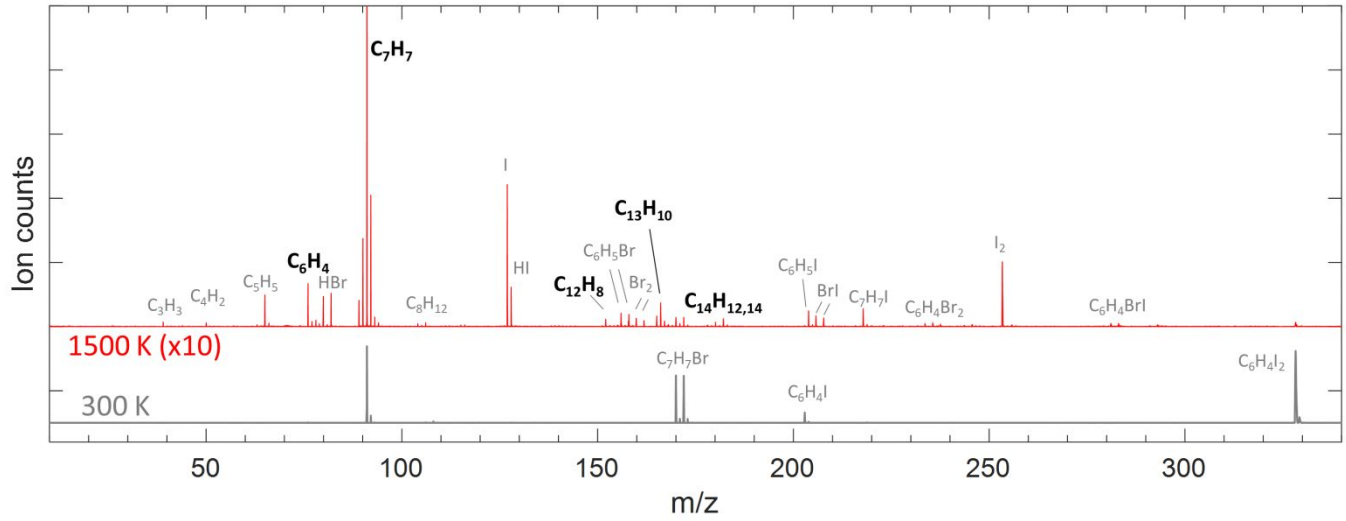

Figure 4. Mass spectra for the C_7H_7 + C_6H_4 reaction at 300 K (black) and 1500 K (red). Species of interest in this study are shown in bold black. Halogen side reactions create large signals due to the large ionization cross section of Br and I atoms.

in the mass spectrum at temperatures around 1000 K and peaks around 1300 K, while the benzyne signal monotonically increases. As for the *o*-C_6H_4 + C_3H_3 reaction described earlier, the linear C_6H_4 isomer may contribute to the total C_6H_4 signal.[50, 51] At temperatures below 1400 K, at which the benzyl radical concentration is highest, the cyclic *o*-benzyne is likely to be the most dominant C_6H_4 isomer. The initial adduct $C_{13}H_{11}$ peaks around 1400 K and its signal is smaller than the $C_{13}H_{10}$ product that is formed following a hydrogen loss after the initial product formation. The drop in the $C_{13}H_{10}$ signal mirrors the drop in the benzyl signal, which suggests that the continuous rise in the C_6H_4 signal above 1400 K may be due to the linear isomer.

According to Matsugi and Miyoshi,[22] the reaction proceeds through the initial 2-benzyl-phenyl radical (see Scheme 2) that can isomerize through reaction barriers below the entrance channel to form hydro-fluorene radical isomers. Fluorene, through H-loss channels, is the predicted $C_{13}H_{10}$ reaction product. The origin of the $C_{13}H_9$ radical cannot be conclusive clarified. This resonance-stabilized radical likely comes from thermal unimolecular dissociation of $C_{13}H_{10}$. The high yield at the highest sampled temperatures of around 1600 K supports this conclusion. However, H-abstraction reactions, potentially from the halogen atoms released by the precursors, cannot be ruled out.

We also plot the signal of $C_{13}H_9$ here because it is a resonance-stabilized radical that is potentially formed through an additional H-loss at these high temperatures (see Scheme 2). In the studied temperature range up to 1600 K, the $C_{13}H_9$ signal increases monotonically.

The comparison of the cross-reaction products $C_{13}H_x$ (x=11-9) to the self-reaction products helps reveal the possible importance of reaction 1. Figure 6 shows that the main cross reaction product, $C_{13}H_{10}$ (*m/z* 166.078) has a substantially larger signal at temperatures above 1300 K than the benzyne self-reaction ($C_{12}H_8$, *m/z* 152.063) or benzyl self-reaction ($C_{14}H_{14}$, *m/z* 182.110 and $C_{14}H_{12}$, *m/z* 180.094) products. At lower temperatures, the benzyne concentration is low while the benzyl self-reaction dominates. Although Kaiser *et al.* discussed $C_{14}H_{10}$ (*m/z* 178.078) isomers as products of the benzyl self-recombination reaction,[38] we did not observe this product,

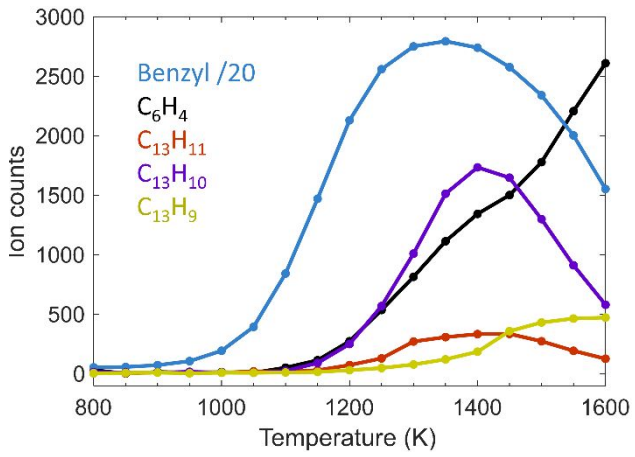

Figure 5. Temperature-dependent ion counts for the reactants C_6H_4 and benzyl are shown together with ions counts for the reaction products $C_{13}H_{11}$, $C_{13}H_{10}$, and $C_{13}H_9$.

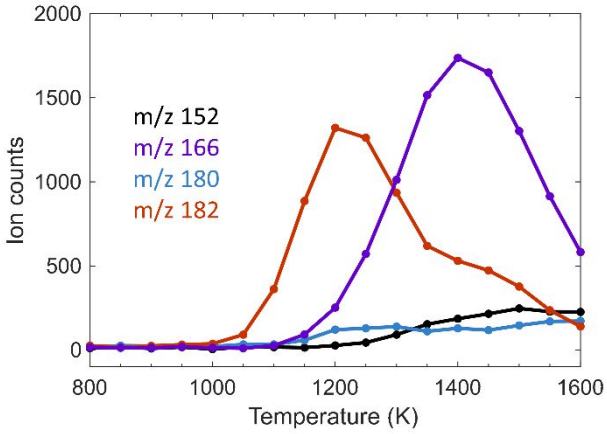

Figure 6. Comparison between self-reactions (m/z = 152.063 and 180.094+182.110) and the main cross-reaction product (m/z = 166.078). The cross reaction is favorable at high temperature.

probably because of the lower benzyl concentration compared to their experiments. All these molecules should have similar ionization cross sections and mass discrimination factors due to the similarity of the masses, and any small differences should not promote $C_{13}H_{10}$ (m/z 166.078) over both higher and lower masses.

Conclusions

More than 10 years ago, Matsugi and Miyoshi theoretically explored the reaction of *o*-benzyne with benzyl radicals as a potential source of PAHs in combustion processes.[22] In this work, we provide the long-awaited experimental evidence of the reactants to indeed form the predicted PAHs efficiently.

What stands out in the chemistry of *o*-C_6H_4 is the efficient ability to form PAHs via diradical addition. That is, in *o*-C_6H_4 chemistry, multiring species are favored over open-chain or aliphatically bridged PAHs. For example, the reaction studied here, *o*-C_6H_4 + C_7H_7, is barrierless and creates an intermediate with a radical site on the aromatic ring, which then allows for a rapid ring closure to yield a five-membered ring structure.

These experimental results support the claim that *o*-benzyne tends to react with resonance-stabilized radicals to produce long-lived polycyclic species. In addition, the comparisons between these cross-reactions of interest and the self-reactions of each of the reactants further supports the possible relevance of such reactants in pyrolysis environments. The benzyne self-reaction is not very fast[47] and the self-reactions of resonance stabilized radicals tend to be highly reversible. In contrast, benzyne reacts readily with these radicals. While the reverse reaction is not directly probed here, it does not appear to be substantially depleting the products.

The *o*-C_6H_4 + C_7H_7 reaction elucidated here provides a versatile concept introducing a five-membered ring structure into polycyclic aromatic systems, i.e., fluorene and the fluorenyl radical. The pentagon-bearing species are important in the growth of PAHs because of their contributions via ring-enlargement reactions to further molecular-weight growth and because PAHs carrying five-membered rings are a critical prerequisite for curved PAHs. In summary, extensive reaction schemes of o-benzyne could lead to curved PAHs.

Author Contributions

DEC and NH conceptualized the experimental work. DEC and MMSM performed the experiments and analyzed the data. DEC and NH prepared the manuscript.

Conflicts of interest

There are no conflicts to declare.

Acknowledgements

DEC and NH acknowledge support from the U.S. Department of Energy, Office of Science, Office of Basic Energy Sciences, Division of Chemical Sciences, Geosciences and Biosciences. DEC additionally acknowledges financial support from the Air Force Office of Scientific Research (AFOSR). MMSM acknowledges support by the Department of Energy, Office of Science, Office of Workforce Development for Teachers and Scientists (WDTS) under the Science Undergraduate Laboratory Internships Program (SULI). Sandia National Laboratories is a multimission laboratory managed and operated by the National Technology and Engineering Solutions of Sandia, LLC, a wholly owned subsidiary of Honeywell International, Inc., for the U.S. DOE's National Nuclear Security Administration under contract DENA0003525. This paper describes objective technical results and analysis. Any subjective views or opinions that might be expressed in this article are those of the authors and do not necessarily represent the official policy or position of the U.S. Air Force Academy, the Air Force, the Department of Energy, the Department of Defense, or the U.S. Government.

References

1 H. H. Wenk, M. Winkler and W. Sander, *Angewandte Chemie International Edition*, 2003, **42,** 502-528.
2 R. v. Stoermer and B. Kahlert, *Berichte der deutschen chemischen Gesellschaft*, 1902, **35,** 1633-1640.
3 C. Wentrup, *Australian Journal of Chemistry*, 2010, **63,** 979-986.
4 A. Comandini and K. Brezinsky, *The Journal of Physical Chemistry A*, 2012, **116,** 1183-1190.
5 H. Jin, W. Yuan, W. Li, J. Yang, Z. Zhou, L. Zhao, Y. Li and F. Qi, *Progress in Energy and Combustion Science*, 2023, **96,** 101076.
6 J. Cernicharo, M. Agúndez, R. Kaiser, C. Cabezas, B. Tercero, N. Marcelino, J. Pardo and P. De Vicente, *Astronomy & Astrophysics*, 2021, **652,** L9.
7 F. Zhang, D. Parker, Y. S. Kim, R. I. Kaiser and A. M. Mebel, *The Astrophysical Journal*, 2011, **728,** 141.
8 A. Comandini, S. Abid and N. Chaumeix, *The Journal of Physical Chemistry A*, 2017, **121,** 5921-5931.
9 G. Porter and J. I. Steinfeld, *Journal of the Chemical Society A: Inorganic, Physical, Theoretical*, 1968**,** 877-878.
10 R. S. Tranter, S. J. Klippenstein, L. B. Harding, B. R. Giri, X. Yang and J. H. Kiefer, *The Journal of Physical Chemistry A*, 2010, **114,** 8240-8261.
11 F. Hirsch, E. Reusch, P. Constantinidis, I. Fischer, S. Bakels, A. M. Rijs and P. Hemberger, *The Journal of Physical Chemistry A*, 2018, **122,** 9563-9571.
12 B. Shukla, K. Tsuchiya and M. Koshi, *The Journal of Physical Chemistry A*, 2011, **115,** 5284-5293.
13 A. Comandini and K. Brezinsky, *The Journal of Physical Chemistry A*, 2011, **115,** 5547-5559.
14 R. G. Miller and M. Stiles, *Journal of the American Chemical Society*, 1963, **85,** 1798-1800.
15 L. Friedman and D. F. Lindow, *Journal of the American Chemical Society*, 1968, **90,** 2324-2328.
16 G. Friedrichs, E. Goos, J. Gripp, H. Nicken, J.-B. Schönborn, H. Vogel and F. Temps, *Zeitschrift für Physikalische Chemie*, 2009, **223,** 387-407.
17 M. N. McCabe, P. Hemberger, E. Reusch, A. Bodi and J. Bouwman, *The Journal of Physical Chemistry Letters*, 2020, **11,** 2859-2863.

18 L. Monluc, A. A. Nikolayev, I. A. Medvedkov, V. N. Azyazov, A. N. Morozov and A. M. Mebel, *ChemPhysChem*, 2022, **23,** e202100758.
19 J. Meinwald and G. W. Gruber, *Journal of the American Chemical Society*, 1971, **93,** 3802-3803.
20 J. Bouwman, M. N. McCabe, C. N. Shingledecker, J. Wandishin, V. Jarvis, E. Reusch, P. Hemberger and A. Bodi, *Nature Astronomy*, 2023, **7,** 423-430.
21 N. Hansen, T. Bierkandt, N. Gaiser, P. Oßwald, M. Köhler and P. Hemberger, *Proceedings of the Combustion Institute*, 2023, **40,** 105623.
22 A. Matsugi and A. Miyoshi, *Physical Chemistry Chemical Physics*, 2012, **14,** 9722-9728.
23 M. Frenklach, *Physical chemistry chemical Physics*, 2002, **4,** 2028-2037.
24 K. O. Johansson, M. P. Head-Gordon, P. E. Schrader, K. R. Wilson and H. A. Michelsen, *Science*, 2018, **361,** 997-1000.
25 R. I. Kaiser and N. Hansen, *The Journal of Physical Chemistry A*, 2021, **125,** 3826-3840.
26 J. W. Martin, M. Salamanca and M. Kraft, *Progress in Energy and Combustion Science*, 2022, **88,** 100956.
27 M. Baroncelli, Q. Mao, S. Galle, N. Hansen and H. Pitsch, *Physical Chemistry Chemical Physics*, 2020, **22,** 4699-4714.
28 L. Zhao, R. I. Kaiser, W. Lu, B. Xu, M. Ahmed, A. N. Morozov, A. M. Mebel, A. H. Howlader and S. F. Wnuk, *Nature Communications*, 2019, **10,** 3689.
29 X. Mercier, A. Faccinetto, S. Batut, G. Vanhove, D. K. Božanić, H. Hróðmarsson, G. A. Garcia and L. Nahon, *Physical Chemistry Chemical Physics*, 2020, **22,** 15926-15944.
30 C. Shao, G. Kukkadapu, S. W. Wagnon, W. J. Pitz and S. M. Sarathy, *Combustion and Flame*, 2020, **219,** 312-326.
31 N. Hansen, J. A. Miller, S. J. Klippenstein, P. R. Westmoreland and K. Kohse-Höinghaus, *Combustion, Explosion, and Shock Waves*, 2012, **48,** 508-515.
32 D. E. Couch, G. Kukkadapu, A. J. Zhang, A. W. Jasper, C. A. Taatjes and N. Hansen, *Proceedings of the Combustion Institute*, 2023, **39,** 643-651.
33 N. Hansen, B. Yang, M. Braun-Unkhoff, A. Ramirez and G. Kukkadapu, *Combustion and Flame*, 2022, **243,** 112075.
34 G. Kukkadapu, S. Wagnon, W. Pitz and N. Hansen, *Proceedings of the Combustion Institute*, 2021, **38,** 1477-1485.
35 B. Adamson, S. Skeen, M. Ahmed and N. Hansen, *The Journal of Physical Chemistry A*, 2018, **122,** 9338-9349.
36 D. E. Couch, A. J. Zhang, C. A. Taatjes and N. Hansen, *Angewandte Chemie International Edition*, 2021, **60,** 27230-27235.
37 J. A. Rundel, C. Martí, J. Zádor, P. E. Schrader, K. O. Johansson, R. P. Bambha, G. T. Buckingham, J. P. Porterfield, O. Kostko and H. A. Michelsen, *The Journal of Physical Chemistry A*, 2023, **127,** 3000-3019.
38 R. I. Kaiser, L. Zhao, W. Lu, M. Ahmed, V. S. Krasnoukhov, V. N. Azyazov and A. M. Mebel, *Nature Communications*, 2022, **13,** 786.
39 D. E. Couch, A. W. Jasper, G. Kukkadapu, M. M. San Marchi, A. J. Zhang, C. A. Taatjes and N. Hansen, *Combustion and Flame*, 2023, **257,** 112439.
40 W. Li, J. Yang, L. Zhao, D. Couch, M. San Marchi, N. Hansen, A. N. Morozov, A. M. Mebel and R. I. Kaiser, *Chemical Science*, 2023, **14,** 9795-9805.
41 D. W. Kohn, H. Clauberg and P. Chen, *Review of Scientific Instruments*, 1992, **63,** 4003-4005.
42 M. Balat-Pichelin and A. Bousquet, *Journal of the European Ceramic Society*, 2018, **38,** 3447-3456.
43 P. J. Weddle, C. Karakaya, H. Zhu, R. Sivaramakrishnan, K. Prozument and R. J. Kee, *International Journal of Chemical Kinetics*, 2018, **50,** 473-480.
44 P. Hemberger, X. Wu, Z. Pan and A. Bodi, *The Journal of Physical Chemistry A*, 2022, **126,** 2196-2210.
45 K. Moshammer, L. Seidel, Y. Wang, H. Selim, S. M. Sarathy, F. Mauss and N. Hansen, *Proceedings of the Combustion Institute*, 2017, **36,** 947-955.
46 L. Ruwe, K. Moshammer, N. Hansen and K. Kohse-Höinghaus, *Physical Chemistry Chemical Physics*, 2018, **20,** 10780-10795.
47 M. E. Schafer and R. S. Berry, *Journal of the American Chemical Society*, 1965, **87,** 4497-4501.
48 L. Zhao, W. Lu, M. Ahmed, M. V. Zagidullin, V. N. Azyazov, A. N. Morozov, A. M. Mebel and R. I. Kaiser, *Science Advances*, 2021, **7,** eabf0360.
49 J. A. Miller and S. J. Klippenstein, *The Journal of Physical Chemistry A*, 2003, **107,** 7783-7799.
50 G. Ghigo, A. Maranzana and G. Tonachini, *Physical Chemistry Chemical Physics*, 2014, **16,** 23944-23951.
51 X. Zhang, A. T. Maccarone, M. R. Nimlos, S. Kato, V. M. Bierbaum, G. B. Ellison, B. Ruscic, A. C. Simmonett, W. D. Allen and H. F. Schaefer, III, *The Journal of Chemical Physics*, 2007, **126**.
52 A. Matsugi, *The Journal of Physical Chemistry A*, 2020, **124,** 824-835.
53 C. Martí, H. A. Michelsen, H. N. Najm and J. Zádor, *The Journal of Physical Chemistry A*, 2023, **127,** 1941-1959.

Data for this article will be made available at the webpage of the “U.S. Department of Energy Office of Scientific and Technical Information” webpage at osti.gov